Haptic-Enhanced Bioimpedance Needle for Precision Navigation in Central Venous Catheterisation with Millimetre Accuracy

Qingyu Zhang[1], Ahmed Al-Hindawi[2], Andreas Demosthenous[1] and Yu Wu[1]

[1]Department of Electronic and Electrical Engineering, University College London, Torrington Place, London WC1E 7JE, UK

[2]Centre for Intensive Care Medicine, University College London, Gower Street, London WC1E 6BT, UK

e-mail: qingyu.zhang.23@ucl.ac.uk; yu.wu.09@ucl.ac.uk

2025 IEEE International Symposium on Circuits and Systems (ISCAS) | 979-8-3503-5683-0/25/$31.00 ©2025 IEEE | DOI: 10.1109/ISCAS56072.2025.11044142

***Abstract*—Central venous catheterisation (CVC) involves the precise and challenging task of needle insertion, which can be difficult and prone to complications. This paper presents a bioimpedance (BIOZ) system for precision needle navigation in CVC. The system integrates BIOZ with a haptic feedback mechanism to assist clinicians during the catheterisation procedure. Four types of embedded needle probes were designed for high-sensitivity BIOZ sensing. The probe integrates with a compact electronic handle system for real-time BIOZ measurement and data communication, enabling real-time tissue classification and haptic feedback for optimal needle positioning. In 24 experimental trials with user participation using a phantom model, the system demonstrated a 100% success rate in venous entry, with a root mean square error (RMSE) of 0.66 mm and an 87% probability of achieving a position within ±1 mm of the vein centre. The compact and portable design ensures compatibility with clinical settings, laying a foundation for future improvements in robotic-assisted CVC and procedures alike.**

Keywords—Bioimpedance needle, central venous catheterisation, haptic-assistive device, human-machine interface, robotic-assisted surgery, venous entry detection.

I. Introduction

Central venous catheterisation (CVC) is an invasive procedure that inserts catheters into large blood vessels for treatments such as drug delivery, chemotherapy, nutrition, and patient monitoring [1]. Annually, 27 million CVC procedures are conducted globally, however, these procedures carry substantial risks, including venous puncture, pneumothorax, and catheter placement failures, leading to complication rates as high as 20% and can cause significant morbidity and mortality [1], [2]. The success of CVC relies heavily on the accurate insertion of the guiding needle into the target area, a crucial step for ensuring effective follow-up interventions, e.g., catheter placement. Current best practice is to use ultrasound (US) guidance to visualise the needle in real-time. However, this technique presents considerable challenges for practitioners [3]. Practitioners must track the needle tip while simultaneously navigating the US probe to visualise the target vessel. Due to the limited field of view of US, this process requires continuous adjustment of both the probe and needle to achieve correct placement. Mastering this technique requires extensive training and supervised practice to ensure proficiency.

Bioimpedance (BIOZ) analysis is an established technique for detecting and differentiating biological tissues [4]. Integrating BIOZ technology with needles that provide real-time feedback could be used to improve US-guided CVC. While the concept of the BIOZ needle has been explored in the literature [5], [6], [7], they are not suitable for CVC-like procedures because:

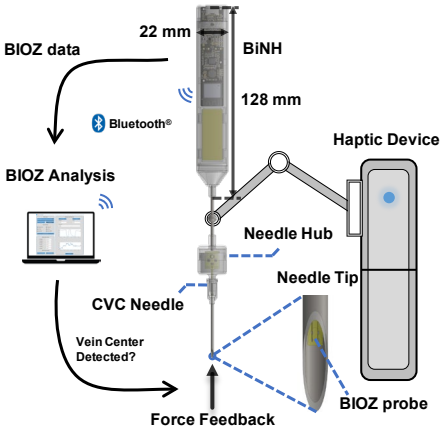

Fig. 1. The integrated BIOZ and haptic-driven needle platform for safe and accurate placement of a central venous catheter (CVC) needle.

1) Electrode design: Most studies adopt commercial electromyography needles with concentric electrodes at the needle tip. This bipolar electrode configuration in BIOZ often introduces an electrode polarisation effect, leading to measurement errors and data instability [6]. In contrast, a tetrapolar BIOZ needle, as reported in [6], eliminates the polarisation effect. However, with a focus on biopsy, the side-mounted electrodes along the needle shaft make it unsuitable for needle navigation, and the fabrication process is complex.

2) Vein centring: Proper needle entry requires the tip to be advanced to the centre of the vein [8]. Incorrect depth – either too shallow or too deep – can complicate the step of guide wire insertion, a step that is crucial for catheter placement during CVC. Achieving consistent centring using only BIOZ data is challenging, leading to the need for multimodality approaches. A dual collaborative robot arm system integrating US and bipolar BIOZ for autonomous venous access was reported in [7]. It achieved a positioning root mean square error (RMSE) less than 1.7 mm under lab conditions. However, this approach could present significant challenges for practical use, including difficulties in completing the subsequent steps of CVC, as well as high costs and regulatory barriers that limit its feasibility for widespread adoption in clinical settings.

This work offers a unique combination of BIOZ and haptic feedback through an integrated platform, as shown in Fig. 1. The needle employs removable probes inserted in the needle for BIOZ measurements, which drive a haptic engine to provide tactile cues for centring the vein along the vertical axis. Unlike the bulky setup of previous systems, this platform is

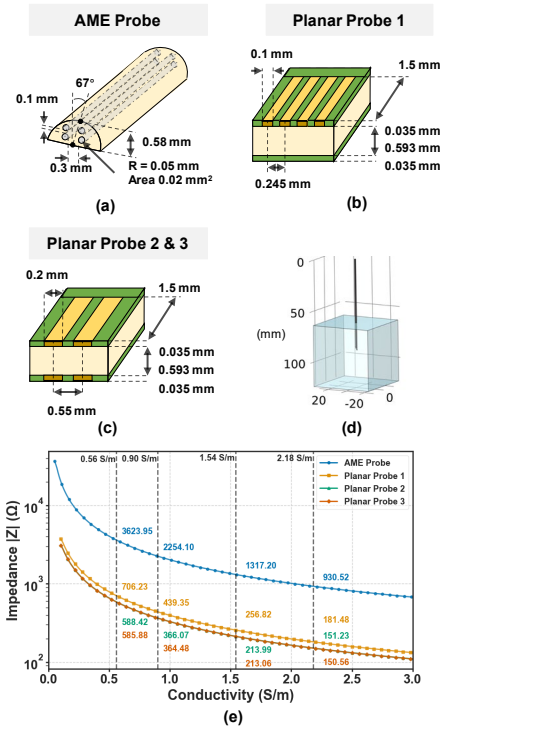

Fig. 2. (a) to (c) show the dimensions of four types of BIOZ probe. (d) 3D model in COMSOL. (e) Simulation results illustrating impedance variations with solution conductivity at 100 kHz. The figure includes annotated reference impedance values at four different conductivities. Impedance reduces as conductivity increases.

compact and portable, integrating all electronics into a wireless BIOZ needle handle (BiNH). The handle is attached to Inverse 3, a haptic device by Haply Robotics (Montreal, Canada), providing an intuitive and remote solution for better needle navigation in CVC.

The rest of the paper is organised as follows. Section II presents the design, modelling, and testing of the tetrapolar sensor probes. Section III describes the design of the BiNH system, haptic integration and the experimental setup. Measurements and discussion are provided in Section IV, followed by conclusion in Section V.

II. Inner BIOZ Probe Design

Direct modifications to the guiding needle, as described in [9], could increase manufacturing complexities and create regulatory hurdles. Alternatively, embedding probes within the needle's hollow shaft is an established practice, offering a more cost-effective and modular solution. In this work, four types of probe were designed and fabricated. One 3D design was fabricated using the next-generation additively manufactured electronic circuits technology (AME) by Nano Dimension (Massachusetts, United States), while the remaining planar probes were realised using printed circuit boards (PCB) for proof-of-concept studies.

A. Modelling of the Tetrapolar BIOZ Probes

The probes employ tetrapolar BIOZ measurements, which use a pair of electrodes to inject current and a pair of electrodes to record the voltage between the subject under test [4]. Fig. 2 (a) illustrates the tip of the AME probe design, which was manufactured with silver electrodes on an acrylic base. Fig. 2 (b) and (c) depict the tip of the planar probes in three variations with a standard gold PCB finish as electrodes. These planar

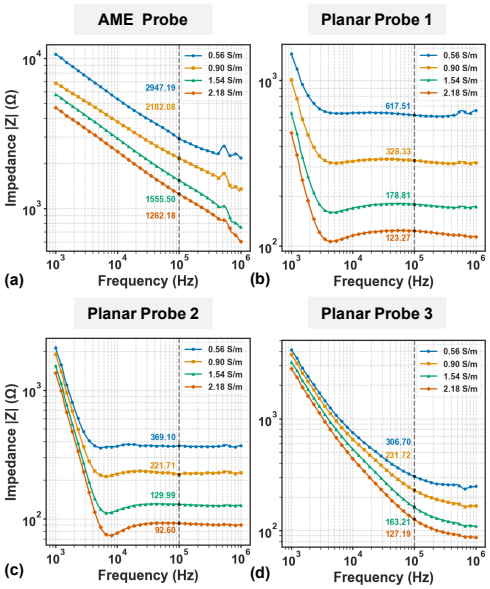

Fig. 3. Electrochemical impedance spectroscopy (EIS) measurements of the four probes in four different saline concentrations. The figure annotates the reference impedance values for an injection current at 100 kHz.

probes also investigate the effects of placing electrodes on one or both sides of the probe, as well as the spatial arrangement of the injection and recording electrodes.

The design was optimised in COMSOL (COMSOL, USA) while considering manufacturing capabilities. The impedance of tissues with different conductivities was calculated by sweeping values from 0.1 S/m to 3.0 S/m, covering a range of tissue types, as illustrated in Fig. 2 (d) and (e). A BIOZ measurement frequency of 100 kHz was chosen in the simulation, as it is commonly used to distinguish between different tissues [10]. Additionally, given the challenges in determining relative permittivity, a blood parameter of 5120 K/m at 100 kHz was used as a constant reference [11]. From the modelling results, the small electrode area of the AME probe resulted in higher impedance, thereby providing a larger dynamic range and improving the signal-to-noise ratio (SNR) of the measurements.

B. EIS Test for Four Types of Probes

Fig. 3 depicts the electrochemical impedance spectroscopy (EIS) measurements over a frequency range of 1 kHz to 1 MHz, acquired using an MFIA impedance analyser (Zurich Instruments, Switzerland). The saline solutions were prepared by dissolving 1.5 g, 2.5 g, 4.5 g, and 6.5 g of salt in 500 ml of deionized water, resulting in conductivities of 0.56 S/m, 0.90 S/m, 1.54 S/m, and 2.18 S/m, respectively, as measured by an HI 8733 conductivity meter (Hanna Instruments, United Kingdom). Although all designs could differentiate between various saline concentrations, the closely matched impedance readouts in the planar probes could make it difficult to identify the subject under test in high-noise environments. In contrast, the AME probe offers improved SNR across the frequency spectrum.

III. System Design and Experiment Setup

Fig. 4 (a) illustrates the complete system structure, which comprises a BiNH, a host laptop, and a haptic device. The BiNH records impedance data from the BIOZ probe, while registering the handle's orientation via the inertial

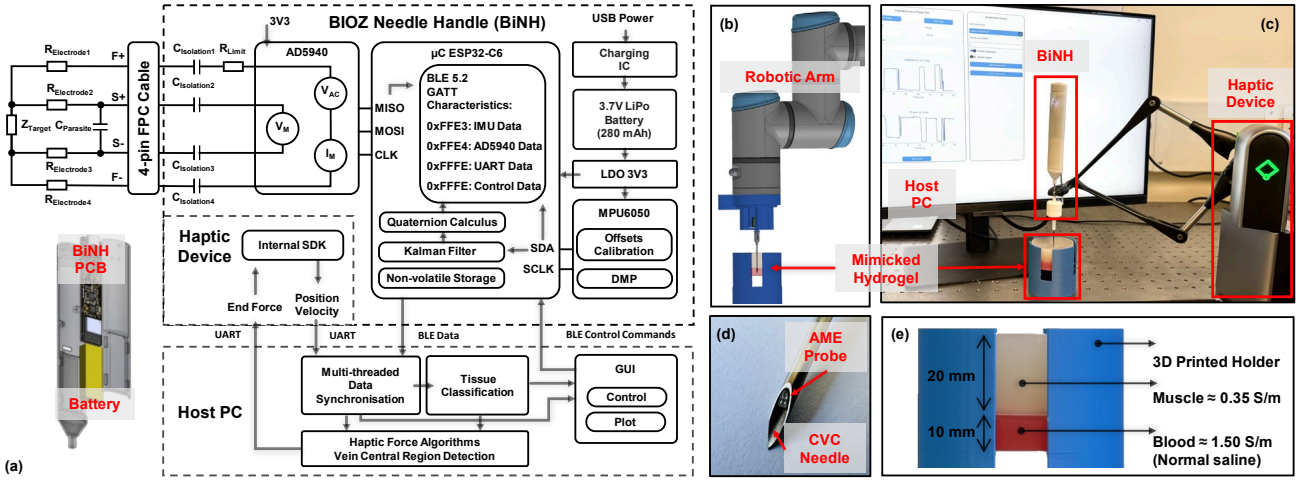

Fig. 4. (a) System architecture of the BiNH with the host computer and haptic device. (b) Robotic arm insertion experimental setup. (c) User-controlled experimental setup. (d) Example of AME probe with CVC needle. (e) Hydrogel test phantom used.

measurement unit (IMU) and transmits the information via Bluetooth low energy (BLE) 5.0 to the host PC. The host PC also records data from the haptic device, together with the BiNH data, to determine the needle insertion distance. Additionally, the host PC synchronises all data for tissue classification and calculates the end force of the haptic device and provides feedback to the user to indicate that the vein's central region is reached.

A. BiNH Circuits

As shown in Fig 4 (a), the BiNH uses a high-precision impedance readout front-end AD5940 (Analog Devices, Massachusetts, United States) to measure BIOZ with its tetrapolar configuration, allowing the system to sample at 800 kbps and internally demodulate impedance via discrete Fourier transform (DFT). The AD5940 outputs impedance data directly in real and imaginary components via SPI communication. In this work, a 400 mV_{pk-pk} sinusoidal signal at 100 kHz was applied, with the DFT operating on 8192 points, resulting in an impedance output frequency of 50 Hz. Through a flexible PCB (FPC) cable, the tetrapolar connection points from the BiNH, namely ±F and ±S, were connected to the BIOZ probe inside the needle hub (see Fig. 1) to form a complete BIOZ needle. With an additional parallel $C_{\text{Parasitics}}$ existing between ±S, the measured impedance can be derived by the following equation:

$$|Z| = \sqrt{\frac{\mathrm{R}_{Target}}{1 + (\omega \cdot \mathrm{R}_{Target} \cdot \mathrm{C}_{Parasitics})^2}} = \frac{V_M}{I_M} \qquad (1)$$

where R_{Target} represents the tissue resistance of interest, $C_{\text{Parasitics}}$ is the parasitic capacitance between ±S, V_M and I_M are the internal measurement values in AD5940. Based on (1), the introduction of $C_{\text{Parasitics}}$ causes a rapid decrease in resistance as the frequency increases. The design also includes the R_{Limit} (1 kΩ) and $C_{Isolution}$ (0.47 pF) components to comply with IEC 60601 standards, aimed at minimising the risks associated with direct current and high current.

This BiNH circuit also incorporates an ESP32-C6 (Espressif, China) and an IMU MPU6050 (InvenSense, TDK, United States), combining its digital motion processor (DMP) with a Kalman filter. The achieved handle orientation estimation is stable and accurate, with drift limited to less than 1 degree at the same orientation after 20 minutes of continuous movement. To balance performance and power consumption, the BLE notification characteristic was set at 30 Hz. The total power consumption is 203.5 mW at full speed, with 178 mW attributed to the BLE chip, allowing up to 5 hours of operation, while in light sleep mode, the power consumption is reduced to 4.5 mW, enabling the system to remain on standby for over ten days.

B. Haptic Device and Host Processing

The host PC integrates two main functions. (1) Tissue classification, based on the thresholding approach, categorises the detected impedance into three types: air, muscle, and blood. (2) Haptic force: as shown in Fig 4 (a), the multi-threaded results are firstly synchronised and passed on to the force feedback algorithm. The total force applied is computed by:

$$\begin{aligned} \overrightarrow{F_{total}} &= m \cdot \overrightarrow{F_{drag}} + n \cdot \overrightarrow{F_{catch}} \\ \overrightarrow{F_{catch}} &= k_s \cdot (\overrightarrow{P_{nearest}} - \overrightarrow{P_{device}}) \\ \overrightarrow{F_{drag}} &= k_d \cdot \overrightarrow{V_{device}} \end{aligned} \qquad (2)$$

where the F_{drag} and F_{catch} are sensation forces applied to simulate the feeling when inserted into tissue; m and n represent force coefficients according to current tissue type, used to adjust the perception of different tissues; k_s and k_d are the drag coefficient and capture stiffness, respectively, and are determined through parameter tuning based on the practical scenario. $P_{nearest}$ refers to the nearest capture grid point, determined using a finely meshed virtual grid to control the device's position within the grid and prevent abnormal forces caused by velocity due to gravitational effects. P_{device} is the device position, and V_{device} is the device's velocity. In summary, the force feedback is determined in real time during the insertion process based on the impedance data and the handle's pose, position, and velocity.

C. Experimental Setup

Fig. 4 (b) shows the first experiment, where a robotic arm UR3e (Universal Robots, United States) drives the discrete BiNH needle system inserted into a hydrogel setup. Detailed in Fig. 4 (e), the muscle hydrogel consists of 15 g agar, 0.6 g salt, and 500 ml water, while the blood hydrogel has 15 g agar, 4.5 g salt, and 500 ml water, stacked to form the test phantom. This planar setup focuses on evaluating the deviation along the vertical axis during insertions. Despite reduced

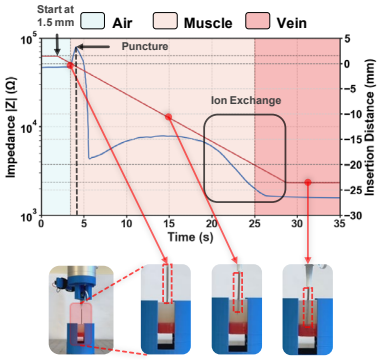

Fig. 5. Impedance (blue curve) and insertion distance (red curve) as functions of time during needle insertion. The sequential images show the needle's position at different time points, corresponding to the red markers on the curves.

conductivity upon solidification, the hydrogel adequately mimics muscle and blood properties. The UR3e insertion speed was programmed to 1 mm/s, with a depth of 25 mm. This experiment aimed to study phenomena at the muscle hydrogel surface and the interface between hydrogel layers for quantitative analysis. The second experiment, depicted in Fig. 4 (c), involved user-controlled needle insertion into the vein centre in three cases: unaided, with impedance-based tissue classification displayed on a graphical user interface (GUI) display, and with combined haptic and impedance guidance. Before the experiment, participants were given instruction only without practice on the device, and the order of cases presented to the participant was randomised to minimise learning biases. Each condition was repeated 24 times, with 8 participants involved, without any prior CVC experience [This study was approved by the Ethics Committee of University College London, ID: 27647/003]. Fig. 4 (d) shows the 16-gauge CVC needle with an AME probe inserted. A more common 18-gauge CVC needle can also be accommodated by scaling the probe accordingly.

IV. Measured Results and Discussion

A. Robotic Arm Insertion Results

Fig. 5 shows the impedance change and the robotic arm's insertion distance as a function of time. At an insertion depth of 0 mm, the needle tip is 'just touching' the gel interface. As insertion increases, impedance rises until a puncture occurs, then drops abruptly and stabilizes once the needle fully crosses the interface. This behaviour results from changes in contact area and insertion force between the hydrogel and the electrode, as well as ion exchange between the hydrogels, which gradually reduces conductivity near the contact surface. Thanks to precise robotic control, the exact point at which the needle enters the blood hydrogel is determined. Upon reaching the final insertion area, stable impedance was observed. These impedance empirical parameters were also used to adjust thresholds for accurately distinguishing between different tissue types in subsequent experiments.

B. User-Handled Insertion Results

Fig. 6 presents the results of user experiments described earlier. The box plots show the end position of the needle tip in each case (no-aid, BIOZ classification, classification with haptic) over 24 trials. Using absolute insertion distance errors, statistical analysis of t-statistics and p-values clearly indicates that the case 3 achieves the highest insertion. Specifically, without any aid, only 68% of trials successfully entered the

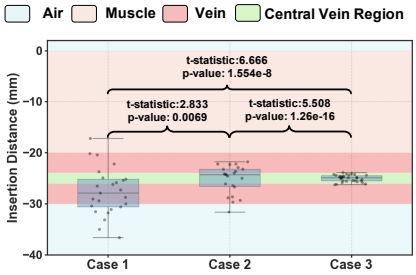

Fig. 6. Final insertion distances in test phantom: case 1 unaided, case 2 with GUI tissue classification, case 3 with both classification and haptic guidance.

vein, which significantly improved to 95.45% with tissue classification, and further to 100% with the addition of haptic feedback. Within the vein region, centring is defined as within ±10% of the vein's 10 mm radius (i.e., ±1 mm from the vein centre), marked with a green bar. Case 3 again achieved the highest vein centring rate of 86.7%, compared to only around 16% for both case 1 and case 2. Based on case 3, the system's navigation precision was calculated to have a standard deviation (σ) of 0.35 mm, a RMSE of 0.66 mm and a mean error (ME) of 0.56 mm along the vertical axis. A performance summary and comparison to other work are shown in Table I. As an assistive device operated by inexperienced users, this system has attained an accuracy range equivalent to that of autonomous systems using high-precision industrial robotics, which integrate more sensory modalities.

TABLE I. Performance Summary and Comparison

References	**This work**	[7]	[12]	[13]	[14]
Application	**CVC**	CVC	PIVC[1]	PIVC	PIVC
Technologies	**BIOZ, Haptic**	US, BIOZ, [2]FS	BIOZ	US, [3]NIR, FS	US, [4]EM, FS
Electrodes	**4**	2	2	N/A	N/A
Insertion Time (s)	**22.0**	N.R.	16.9	N.R.	90±30
Robotic Automation [15]	**Assistive**	Autonomous	Semi-Auto	Autonomous	Autonomous
Vein Entry Failure Rate	**0%**	0%	14±4.9%	0%	13%
σ (mm)	**0.35**	0.52	N.R.	N.R.	N.R.
RMSE (mm)	**0.66**	1.71	N.R.	0.4±0.2	N.R.
ME (mm)	**0.56**	N.R.	N.R.	N.R.	0.23± 0.17

[1]PICV: peripheral intravenous catheterization; [2]FS: force sensing; [3]NIR: near infrared; [4]EM: electromagnetic positioning; N/A: not applicable; N.R.: not reported

V. Conclusion

This paper presented a unique BIOZ-guided haptic needle system for CVC procedures. To better facilitate the embedded tetrapolar measurement, four probes, including a high SNR AME probe, have been designed and validated to distinguish different conductivities. The compact, portable system is capable of real-time BIOZ analysis and needle orientation tracking and is integrated with a haptic device for CVC studies. The system demonstrated a 100% success rate in vein entry and an 87% vein centring rate across 24 experimental trials on phantoms, with a vertical insertion RMSE of 0.66 mm. These results suggest that the system could be a valuable assistive platform for CVC procedures, leading to faster yet more reliable procedures that directly benefit both patients and medical professionals.

REFERENCES

[1] M. Mer, "Central venous catheter-related infection – back to basics," *Afr. J. Thorac Crit Care Med*, vol. 28, no. 1, pp. 5–6, Apr. 2022.

[2] M. Lennon, N. Zaw, D. Pöpping, and M. Wenk, "Procedural complications of central venous catheter insertion", *Minerva Anestesiol.*, vol. 78, Jun. 2012.

[3] B. Saugel, T. W. L. Scheeren, and J.-L. Teboul, "Ultrasound-guided central venous catheter placement: a structured review and recommendations for clinical practice", *Critical Care*, vol. 21, no. 1, p. 225, Aug. 2017.

[4] Y. Wu, F. F. Hanzaee, D. Jiang, R. H. Bayford, and A. Demosthenous, "Electrical impedance tomography for biomedical applications: Circuits and systems review", *IEEE Open J. Circuits Syst.*, vol. 2, pp. 380–397, 2021.

[5] Z. Cheng, B. L. Davies, D. G. Caldwell, and L. S. Mattos, "A new venous entry detection method based on electrical bio-impedance sensing", *Ann. Biomed. Eng.*, vol. 46, no. 10, pp. 1558–1567, Oct. 2018.

[6] J. Park, W.-M. Choi, K. Kim, W.-I. Jeong, J.-B. Seo, and I. Park, "Biopsy needle integrated with electrical impedance sensing microelectrode array towards real-time needle guidance and tissue discrimination", *Sci. Rep.*, vol. 8, no. 1, p. 264, Jan. 2018.

[7] M. Koskinopoulou, A. Acemoglu, V. Penza, and L. S. Mattos, "Dual robot collaborative system for autonomous venous access based on ultrasound and bioimpedance sensing technology", in *2023 IEEE Int. Conf. Robotics Automation (ICRA)*, London, UK, May 2023, pp. 4648–4653.

[8] R. N. Smith and J. P. Nolan, "Central venous catheters", *BMJ*, vol. 347, Nov. 2013.

[9] Y. Hu, C. Limpabandhu, T. Barrett, and Z. T. H. Tse, "Bioimpedance sensing and ablation needles for image-guided therapy", *IEEE Access*, vol. 12, pp. 80859–80871, 2024.

[10] C. Carpano Maglioli, D. G. Caldwell, and L. S. Mattos, "A bioimpedance sensing system for in-vivo cancer tissue identification: Design and preliminary evaluation", in *2017 39th Annual Int. Conf. IEEE Eng. Medicine Biology Society (EMBC)*, Seogwipo, South Korea, Jul. 2017, pp. 4235–4238.

[11] "Dielectric Properties of Body Tissues: HTML clients," *niremf.ifac.cnr.it*. http://niremf.ifac.cnr.it/tissprop/htmlclie/htmlclie.php

[12] Z. Cheng, B. L. Davies, D. G. Caldwell, and L. S. Mattos, "A hand-held robot for precise and safe PIVC", *IEEE Robot. Autom. Lett.*, vol. 4, no. 2, pp. 655–661, Apr. 2019.

[13] M. L. Balter, A. I. Chen, T. J. Maguire, and M. L. Yarmush, "The system design and evaluation of a 7-DOF image-guided venipuncture robot", *IEEE Trans. Robot.*, vol. 31, no. 4, pp. 1044–1053, Aug. 2015.

[14] J. M. Leipheimer *et al.*, "First-in-human evaluation of a hand-held automated venipuncture device for rapid venous blood draws", *Technology*, vol. 07, no. 03n04, pp. 98–107, Sep. 2019.

[15] M. Koskinopoulou, Z. Cheng, A. Acemoglu, D. G. Caldwell, and L. S. Mattos, "Robotic devices for assisted and autonomous intravenous access", *IEEE Trans. Med. Robotics Bionics* vol. 5, no. 2, pp. 170–179, May 2023.